Journal of Soils and Sediments (2019) 19:3832–3846
https://doi.org/10.1007/s11368-019-02313-7

SOILS, SEC 5 • SOIL AND LANDSCAPE ECOLOGY • RESEARCH ARTICLE

Correlation between shear strength and soil physicochemical properties of different weathering profiles of the non-eroded and collapsing gully soils in southern China

Bifei Huang[1] · Ming Qiu[1] · Jinshi Lin[1] · Jialin Chen[1] · Fangshi Jiang[1] · Ming-kuang Wang[1] · Hongli Ge[1] · Yanhe Huang[1]

Received: 30 July 2018 / Accepted: 13 March 2019 / Published online: 30 April 2019

Abstract

Purpose Collapsing gully erosion is a specific form of soil erosion that is widely distributed in the hilly granitic region of tropical and subtropical southern China and resulted in extremely rapid water and soil loss. The aim of this study was to investigate the correlations between soil physicochemical and shear properties and the clay mineralogical of different profiles of the non-eroded soils (without soil erosion) and collapsing gully soils in Changting County, Fujian Province, southeastern China.

Materials and methods A total of 32 sampling soils collected from four pedons of non-eroded and collapsing gully soils were subjected to conventional soil analyses for physicochemical properties. The soil shear strength of collected soils was measured using a triaxial shear apparatus according to the unconsolidated-undrained (UU) method. The clay mineralogical of different profiles soils was examined with an X-ray diffraction (XRD) analysis.

Results and discussion The results showed that non-eroded soils had superior physicochemical characteristics. The cohesive force of the non-eroded soils was generally greater than that of collapsing gully soils. The XRD patterns of the clay fraction indicated that kaolinite, illite, hydroxy-interlayered vermiculite (HIV), and gibbsite were the dominant clay minerals in the studied soils. Pearson's correlation analysis showed that the cohesive force of the studied soils had significant and positive correlations with CEC, exchangeable $Al^{3+} + H^{+}$, Fe_d, Al_d, and Fe_t; the correlation coefficients (R value) for cohesive force were greater than those of internal friction angle. The stepwise multiple linear regression analyses indicated that exchangeable $Al^{3+} + H^{+}$ and Al_d were the dominant factors affecting cohesive force.

Conclusions Compared with collapsing gully soils, non-eroded soils had superior physicochemical and shear properties, indicating that non-eroded soils were better able to resist soil erosion. The findings obtained in the present study were of fundamental significance in understanding the correlation between shear strength and the soil physicochemical properties in the non-eroded soils and collapsing gully soils of tropical and subtropical China.

Keywords Cohesive force · Collapsing gully · Kaolinite · Shear properties · Triaxial shear apparatus

1 Introduction

In the hilly granitic region of tropical and subtropical southern China, a serious type of soil erosion called collapsing gully erosion occurs on hill slopes covered by a thick granite weathering mantle and had been given the local name "Benggang" (Xu 1996; Jiang et al. 2014) or permanent gully (Lin et al. 2015) (Fig. 1a). The concept of a collapsing gully was first proposed by Zeng in 1960, in which composite erosion forms via hydraulic scouring and gravitational collapse (Zeng 1960). These particular types of gullies are generally composed of an upper catchment, collapsing wall, colluvial deposit, scour channel, and alluvial fan (Fig. 1b). According to a national survey by the Monitoring Center of Soil and Water Conservation of China, more than 239,100 permanent gullies are present in the granitic red clay soil regions of southern China, which includes the seven provinces of Guangdong, Guangxi, Jiangxi, Hubei, Fujian, Hunan, and Anhui (Jiang

Responsible editor: Lu Zhang

Electronic supplementary material The online version of this article (https://doi.org/10.1007/s11368-019-02313-7) contains supplementary material, which is available to authorized users.

✉ Yanhe Huang
yanhehuang@163.com

[1] College of Resources and Environment, Fujian Agriculture and Forestry University, Fuzhou 350002, Fujian Province, China

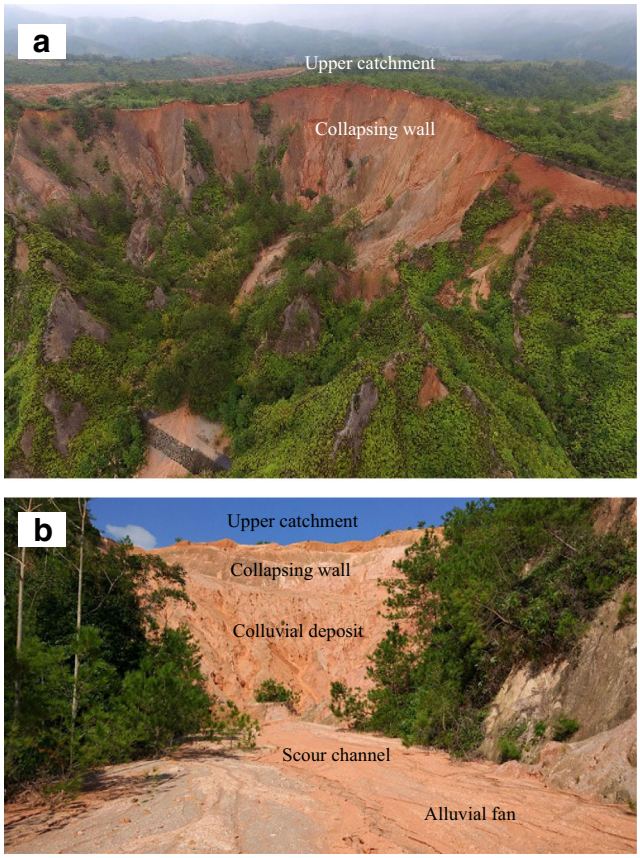

Fig. 1 A typical collapsing gully in Fujian Province. **a** Aerial photo of a collapsing gully in the study area. **b** Upper catchment, collapsing wall, colluvial deposit, scour channel, and alluvial fan

et al. 2014). These gullies develop quickly and forcefully, with an annual average rate of erosion of over 50 kt km^2 yr^{-1} in these areas, which is more than 50-fold faster than the rate of erosion on gentler slopes or on slopes covered with high vegetation. From 1950 to 2005, gully erosion affected 1220 km^2 of land in the granitic red clay soil region, leading to the loss of more than 60 Mt of soil (Zhong et al. 2013). These gullies cause soil loss, downstream aggregation, and increase degradation of agroecological systems; thus, increasing research is focusing on gully erosion.

Most of the relevant research in recent decades focused on the mechanisms of collapsing gully formation (Xu 1996; Luk et al. 1997a; Munro and Huang 1997; Woo et al. 1997); the factors influencing collapsing gully erosion, including variations in the soil physical properties of different soil profiles of collapsing gully walls (Xu 1996; Luk et al. 1997b; Xia et al. 2015); and monitoring of the water and sediment yield from collapsing gullies in the hilly granitic regions (Luk et al. 1997b; Lin et al. 2018). Numerous factors have been considered responsible for collapsing gully development, such as slope steepness and aspect, geology, precipitation, vegetation, and human activity (Liggitt and Fincham 1989; Kakembo et al. 2009; Le Roux and Sumner 2012; Vincent 2013). The slope steepness, aspect, and altitude can affect the scale and rate of collapsing gully development (Xu 1996; Ge et al. 2007). Additionally, low vegetation coverage and unreasonable human activities can induce or promote the development of collapsing gully (Prosser and Slade 1994; Xu 1996). Finally, parent rock characteristics and geological structure can also considerably affect collapsing gully formation. Granite is widely distributed in southern China with a humid tropical climate, and thus a well-developed, thick weathering mantle, which provides the material basis for collapsing gully development, while intense rainfall in the tropical monsoon climate acts as a powerful driver of collapsing gully. More than 85% of collapsing gullies have occurred on granite, while a few are on glutenite, phyllite, and basalt (Ge et al. 2007). Geotechnical properties, such as the physicochemical and mechanical characteristics of rock and soil inherited from the parent rock, are important factors contributing to collapsing gully (Imarhiagbe and Williams 2014; Okunlola et al. 2014; Okengwo et al. 2015).

Soil shear strength represents the soil's ability to resist shearing under the influence of external forces. Two soil shear strength parameters (cohesion force (c) and internal friction angle (φ)) are important factors associated with soil collapse (Lohnes and Handy 1968; Hessel and Van Asch 2003). Rainfall is abundant in the red soil region of southern China. The soil shear strength of collapsing wall decreases after adsorbing water, which results in the instability of the collapsing wall and can cause further collapse. Therefore, the moisture characteristic is closely related to the formation of a collapsing gully and also regarded as a critical factor affecting soil shear strength (Xu 1996; Dong et al. 2011; Lin et al. 2013). Lin et al. (2013) analyzed the regularity of shear strength with soil moisture content in different soil layers with a triaxial shear test; the result indicated that with increasing moisture content, cohesive forces showed a trend of initial increase and then a decrease, while the internal friction angle decreased with increasing moisture content. The same results were reported by Wei et al. (2018), while they studied to determine how indicators of soil shear strength vary with the soil water content and dry density.

However, correlation between shear strength and soil physicochemical properties of different weathering profiles of the non-eroded and collapsing gully soils in southern China with a triaxial shear apparatus still remained obscure. Therefore, two different non-eroded soils were collected from the towns of Sidu (SD) and Tongfang (TF) without collapsing gully erosion and other two soil pedons were collected from collapsing gullies from the town of Hetian (HT) in Changting County, Fujian Province, southeastern China. The aims of the present study were to (1) identify the similarities and differences in soil physicochemical and mineralogical properties of different weathering profiles in the non-eroded and collapsing gully soils, (2) investigate the shear strength (cohesive force and

internal friction angle) with a triaxial shear apparatus in the four pedons of 32 soil samples, and (3) study the correlations between shear strength (cohesive force and internal friction angle) and soil physicochemical properties by analyzing the status and variation in shear strength.

2 Materials and methods

2.1 Study area

Fujian Province is located in southeastern China, and Changting County is located in southwestern Fujian Province. The county is located within the latitudes of 25° 18′ 40″N to 26° 02′ 05″N, and the longitudes of 116° 00′ 45″E to 116° 39′ 20″E in a subtropical region. The climate in this region is humid, with a mean annual air temperature of 17.5–18.8 °C and a mean annual precipitation of 1737.1 mm, 71.9% of which occurs from April to September. The natural vegetation at the sites consists of *Pinus massoniana*, shrubs, weeds, and secondary vegetation. Changting County covers an area of 3099 km^2 and is underlain by granitoid rocks and metamorphosed equivalents. In geological history, Changting County was part of a shallow sea and coastal location in a subtropical monsoon climate with abundant rainstorms and a highly complex geological structure. The Changting basin is a residual sedimentary basin consisting of Upper Triassic to Lower-Middle Jurassic strata, which are compressed into NNE-striking folds. The Upper to Lower Jurassic sedimentary rock series consists of conglomerates and sandstones, while the Middle Jurassic series consists of fine- to medium-grained quartz sand and silt stones. The folded layer is intruded by a granitic pluton (Xu et al. 2011). However, most of the soil parent material of Changting County is coarse-grained biotite granite, which consists of quartz, plagioclase, K-feldspar, and biotite. In granite areas, tropical weathering of the granite often produces a deep weathering profile that occasionally reaches depths of more than 50 m, and the regolith consists of quartz grains and felsic clay minerals (Sheng and Liao 1997). The weathered materials are easily eroded, which give rise to mass wasting and erosion by rain and runoff on steep slopes when protective vegetative covering is removed (Luk et al. 1997a). After several wet-dry cycles, deep and wide cracks are easily formed, triggering gully erosion.

2.2 Soil samplings

Two pedons of non-eroded soils were sampled from the towns of Sidu (SD; pedon I) and Tongfang (TF; pedon II), and other two pedons of the collapsing gully soils were sampled from the town of Hetian (HT; pedon III and pedon IV) in Changting County (Fig. 2). According to the height of weathering profiles of the soils, the soil samples were collected from two non-eroded soil pedons (pedon I and pedon II) and were separated into 7 and 6 soil horizons, respectively; 11 and 8 soil samples were collected from two collapsing gullies (pedon III and pedon IV), respectively, with a total of 32 sampling soils. The information of soil sample sites and soil sampling depth is presented in Table 1.

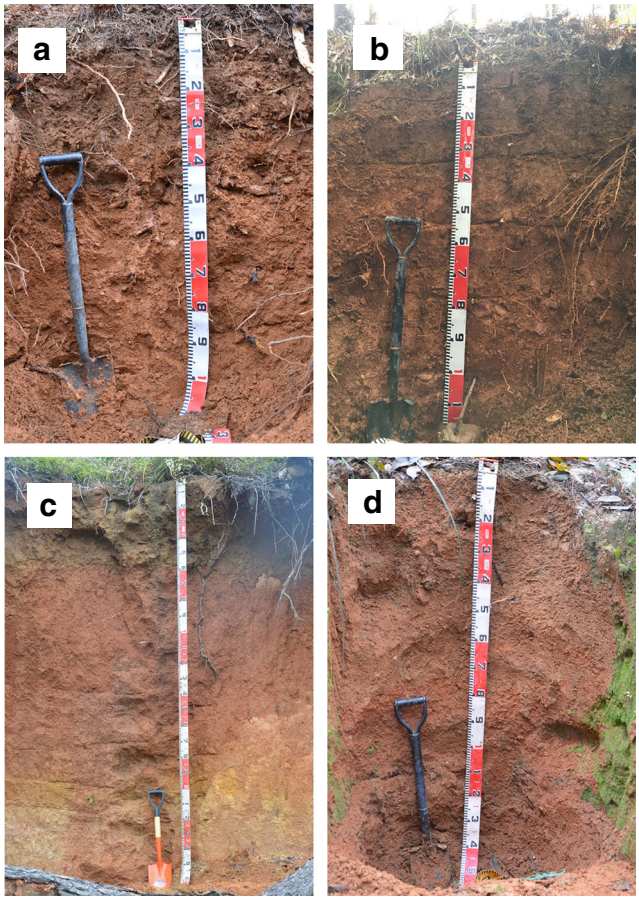

Fig. 2 Sampling sites: **a** pedon I, **b** pedon II, **c** pedon III, and **d** pedon IV

2.3 Soil analyses

The bulk samples of each soil were air-dried at room temperature and ground to pass through a 2-mm sieve. The pHs of the bulk soils (< 2 mm) were measured at a soil to water ratio of 1:2.5 using a pH meter (STARTER 2100, OHAUS Instruments Co., Ltd., Shanghai, China). The particle size distribution of the soil samples was measured using a Laser Granulometer (BT-9300ST, Bettersize Instruments Ltd., Liaoning, China). Soil organic matter (SOM) was determined with wet-oxidation method (Jackson 1979). The cation-exchange capacity (CEC) and exchangeable cations (K, Na, Ca, and Mg) in the soils were determined using the ammonium acetate method buffered at pH 7 (Rhoades 1982), and the concentrations of exchangeable K, Na, Ca, and Mg were determined with an inductively coupled plasma optical emission spectrometer (ICP-OES) (Optima 8000, PerkinElmer, New

Table 1 Descriptions of the pedons I, II, III, and IV

Location	Latitude	Longitude	Sample	Depth (cm)	Moist color	Description	RI[a]
Sidu (SD)	25° 40′ 41″N	116° 12′ 29″E	I-A	0–10	7.5YR3/1	Root (50%)	0.83
			I-B_1	10–30	7.5YR4/4	Root (20%)	2.50
			I-B_2	30–45	7.5YR5/4	Subangular	2.00
			I-B_3	45–70	7.5YR5/6	Subangular	3.00
			I-B_4	70–90	7.5YR5/6	Subangular	3.00
			I-B_5	90–105	7.5YR5/8	Subangular	4.00
			I-C	> 105	7.5YR5/6	Subangular	3.00
Tongfang (TF)	25° 47′ 25″N	116° 35′ 01″E	II-A	0–10	7.5YR4/4	Root (50%)	2.50
			II-AB	10–30	7.5YR4/6	Subangular	3.75
			II-B_1	30–50	7.5YR5/6	Subangular	3.00
			II-B_2	50–78	7.5YR5/8	Subangular	4.00
			II-B_3	78–100	7.5YR5/6	Subangular	3.00
			II-B_4	> 100	7.5YR5/6	Subangular	3.00
Hetian (HT)	25° 39′ 21″N	116° 28′ 08″E	III-A	0–8	7.5YR3/2	Root (80%)	1.67
			III-B_1	8–24	5YR5/3	Subangular	3.00
			III-B_2	24–61	5YR5/4	angular	4.00
			III-B_3	61–94	2.5YR5/6	angular	9.00
			III-B_4	94–143	2.5YR4/6	angular	11.25
			III-B_5	143–177	2.5YR5/6	angular	9.00
			III-B_6	177–203	2.5YR5/6	angular	9.00
			III-B_7	203–222	7.5YR6/6	Subangular	2.5
			III-B_8	222–254	7.5YR7/6	Subangular	2.14
			III-B_9	254–278	7.5YR8/6	Subangular	1.88
			III-C	> 278	7.5YR7/2	Gravel (80%)	0.71
Hetian (HT)	25° 35′ 52″N	116° 27′ 39″E	IV-A	0–7	7.5YR4/2	Root (80%)	1.25
			IV-AB	7–15	7.5YR5/4	Root (40%)	2.00
			IV-B_1	15–32	7.5YR5/6	Subangular	3.00
			IV-B_2	32–59	7.5YR5/6	angular	3.00
			IV-B_3	59–81	7.5YR5/6	angular	3.00
			IV-B_4	81–100	7.5YR5/6	angular	3.00
			IV-B_5	100–125	7.5YR5/8	angular	4.00
			IV-B_6	> 125	7.5YR5/6	angular	3.00

[a] RI redness index [(10 − hue) × chroma / value] (Aniku and Singer 1990)

York, NY). Base saturation and exchangeable Al^{3+} + H^+ concentrations were calculated and estimated as (K + Na + Ca + Mg) / CEC × 100% (Jackson 1979). Free Fe-, Al-, Si-, and Mn-oxides (Fe_d, Al_d, Si_d, and Mn_d) were extracted with dithionite-citrate-bicarbonate (DCB) solutions (Mehra and Jackson 1960); X-ray non-crystalline Fe-, Al-, Si-, and Mn-oxides (Fe_o, Al_o, Si_o, and Mn_o) were extracted with pH 3 ammonium oxalate solution (0.2 M) (Schwertmann 1964), and organically bound Fe-, Al-, Si-, and Mn oxides (Fe_p, Al_p, Si_p, and Mn_p) were treated with 0.1 M Na-pyrophosphate solution (McKeague et al. 1971). Total soil Fe (Fe_t) was determined after digestion with hydrofluoric acid and aqua regia solutions. The concentrations of extracted Fe-, Al-, Si-, and Mn-oxides and Fe_t were determined using ICP-OES. All chemicals were reagent grade, and all experiments were conducted in triplicate.

2.4 Soil shear strength tests

The soil cohesive force and internal friction angle were measured using the triaxial shear strength test. A triaxial shear apparatus (TKA-TTS-3N, Nanjing TKA Technology Co., Ltd., Shanghai, China) was used to conduct the shear strength test according to the unconsolidated-undrained (UU) method. The water content of the soil samples was controlled according to the natural bulk density in a cylindrical mold (diameter 31.9 mm, height 80 mm) and uniformly tamped with a rod. The water content of the remolded specimen and the test temperature were held at 15% and 25 °C, respectively. The UU shear strength triaxial tests were performed under three cell pressures with 50, 100, and 200 kPa, and sheared with a strain rate of 0.4 mm min^{-1}.

2.5 X-ray diffraction

Soil samples were pretreated with 30% H_2O_2 to remove organic matter and treated with DCB to remove iron-oxide coatings. Then, the soil samples were dispersed using a 5% sodium hexametaphosphate solution and stirred, and following settling for 8 h, the clay minerals were extracted according to Stokes' law. For improved identification of soil clay minerals by X-ray diffraction (XRD) analysis, clays were dispersed in H_2O and separated by centrifugation. The silt was separated from the sand by wet sieving (53-μm sieve). All fractions (sand, silt, and clay) were freeze dried.

The tested samples were saturated with Mg-glycerol (Mg-gly) and potassium (K). The Mg saturation of various samples was examined at 25 °C before and after glycerol solvation. The K-saturation of various samples was examined by XRD analysis at 25 °C before and after heating at 110, 250, 350, 450, and 550 °C for 2 h (Jackson 1979; Pai et al. 1999). The oriented clay specimens were examined with an X-ray diffractometer (Ultima IV, Rigaku Corporation, Tokyo, Japan) using Cu-Kα radiation (λ = 1.5418 Å) generated at 40 kV and 40 mA. Diffraction patterns were recorded in the range of 2θ = 3 to 40° with a scanning speed of 1° 2θ min^{-1}. The random powder XRD patterns of the silt and sand fractions were scanned from 3 to 60° 2θ at 1° 2θ min^{-1}. Semi-quantitative estimations of clay minerals were performed according to the methods of Brindley (1980) and Pai et al. (1999).

2.6 Scanning electron microscopy

Morphological studies of clay samples were performed with a scanning electron microscope (Phenom ProX, Phenom-World, Netherlands). A conductive double-sided adhesive was pasted onto clay powder samples. Then, the samples were coated with gold using a sputter coater prior to scanning.

2.7 Statistical analyses

A one-way analysis of variance (ANOVA) was performed to examine the effects of soil depth on soil physicochemical properties and soil shear properties. Pearson's correlation analysis was performed to correlate the soil physicochemical properties across soil depth in the different pedons with shear properties. Regression analysis was used to analyze the relationships between the soil shear properties and the soil parameters. All tests were performed using the statistical program, SPSS 18.0. Figures were prepared in Origin 7.5.

3 Results

3.1 Descriptions of studied soils

The characteristics of each soil horizon are summarized in Table 1. The moist color and redness index [(10 − hue) × chroma / value] showed some variations in the four pedon soils (Table 1) (Aniku and Singer 1990). Homogeneous lateritic soils were classified as red soils according to their moist color, the red pedon was presented with diffuse horizon boundaries of soil features and redness indices, and the gravel soil layers were found at a depth of > 278 cm and redness indices (e.g., RI = 0.71), indicating that the degree of weathering varies with soil depths. Compared with non-eroded soils, the RI of collapsing gully pedon soils had slight high redness indices, indicating that the collapsing gully soils suffer high-degree weathering than non-eroded soils.

3.2 Soil physical and chemical properties

The chemical and physical properties of the studied pedons are summarized in Table 2. The pH of non-eroded and collapsed soils ranged from 4.42 to 5.09 and from 4.46 to 5.48, respectively. The CEC of non-eroded and collapsed soils ranged from 4.34 to 12.96 cmol kg^{-1} and from 2.82 to 10.80 cmol kg^{-1}, respectively. In general, the SOM in each pedon decreased with increasing soil depth due to the humification of litter from the vegetative cover in the upper soil layers and indirectly from root exudate contributions to SOM content. The base saturation and exchangeable cations (K, Na, Ca, and Mg) ranged from 1.47 to 8.69% in the non-eroded soils and from 2.03 to 8.41% in the collapsed soils with low exchangeable Ca, Mg, K, and Na. The exchangeable Al^{3+} + H^{+} concentrations ranged from 4.08 to 12.69 cmol kg^{-1} in the non-eroded soils and from 2.66 to 10.43 cmol kg^{-1} in the collapsed soils. The texture of the non-eroded soils was silt loam, and almost all of the collapsed soils ranged from loam to sandy loam, except pedon III-B_3.

The concentrations of Fe-, Al-, Si-, and Mn-oxides in all pedons are presented in Table 3. The concentrations of free Fe-oxide (Fe_d) of the non-eroded soils ranged from 33.09 to 39.51 g kg^{-1}, while the concentrations in the collapsed soils ranged from 1.87 to 23.71 g kg^{-1}. The concentrations of Al-oxides (Al_d) were ranged from 6.89 to 11.46 g $kg^{-1}$and 1.71 to 5.80 g kg^{-1} of non-eroded and collapsed soils, respectively. Both of Fe_d and Al_d of the non-eroded soils were greater than in the collapsed soils, and the concentrations of free Fe-, Al-, Si-, and Mn-oxides were always greater than those of X-ray non-crystalline and organically bound Fe-, Al-, Si-, and Mn oxides, especially for Fe_d and Al_d. However, the amounts of Si_d, Mn_d, Si_o, Mn_o, Si_p, and Mn_p did not differ considerably between the non-eroded and collapsed soils.

Concentrations of Fe_t in the non-eroded soils ranged from 46.63 to 65.10 g kg^{-1}, and those in the collapsed soils ranged from 3.99 to 30.20 g kg^{-1}, indicating greater amounts of Fe_t in the non-eroded soils than in the collapsed soils. The proportion of crystalline Fe oxides (Fe_c) was calculated according to the difference in the amount of Fe extracted by DCB and by acid ammonium oxalate solution (Fe_d − Fe_o) × 100% / Fe_d (Table 3). The proportions of Fe_c ranged from 94.12 to 99.19% in the non-eroded soils and from 80.25 to 97.06% in the collapsed soils, indicating that the non-eroded soils had slightly higher proportions of Fe_c than that in the collapsed soils.

Table 2 Physical and chemical properties of the studied pedons

Sample	Depth cm	pH (soil:H_2O = 1:2.5)	CEC cmol kg^{-1}	SOM	Exchangeable cation					BS	Sand	Clay	Texture
					K	Na	Ca	Mg	$Al^{3+} + H^+$				
				g kg^{-1}	10^{-3} cmol kg^{-1}				cmol kg^{-1}	%			
I-A	0–10	4.42 ± 0.055 d	12.96 ± 0.89 a	25.33 ± 0.073 a	121.62 ± 2.71 a	6.91 ± 2.49 c	59.86 ± 2.88 a	82.68 ± 0.10 a	12.69 ± 0.89 a	2.10 ± 0.16 ab	18.68 ± 1.78 a	10.38 ± 0.39 d	SiL
I-B_1	10–30	4.43 ± 0.015 d	11.01 ± 1.86 bc	19.67 ± 0.024 b	108.83 ± 0.95 b	8.93 ± 3.72 bc	52.73 ± 3.82 b	75.11 ± 1.03 c	10.77 ± 1.86 bc	2.27 ± 0.38 a	15.91 ± 0.45 b	12.00 ± 0.15 c	SiL
I-B_2	30–45	4.56 ± 0.046 c	10.83 ± 0.30 bc	11.07 ± 0.024 c	90.42 ± 3.06 c	8.8 ± 5.94 bc	54.40 ± 0.74 ab	78.31 ± 0.32 b	10.60 ± 0.31 bc	2.14 ± 0.14 ab	15.84 ± 0.52 c	13.61 ± 0.12 b	SiL
I-B_3	45–70	4.62 ± 0.010 bc	11.74 ± 1.52 ab	8.55 ± 0.024 d	88.33 ± 0.99 c	17.34 ± 9.7 ab	41.55 ± 2.54 c	69.51 ± 1.64 d	11.52 ± 1.53 ab	1.87 ± 0.32 ab	14.73 ± 0.67 bc	13.77 ± 0.31 ab	SiL
I-B_4	70–90	4.64 ± 0.035 b	11.84 ± 0.16 ab	8.21 ± 0.13 e	75.69 ± 0.36 e	7.23 ± 0.98 c	39.88 ± 6.53 c	51.19 ± 0.29 e	11.67 ± 0.17 ab	1.47 ± 0.074 c	15.36 ± 0.72 b	14.21 ± 0.18 a	SiL
I-B_5	90–105	4.93 ± 0.021 a	9.21 ± 0.50 c	7.51 ± 0.061 g	83.48 ± 2.95 d	25.63 ± 2.88 a	36.39 ± 1.94 c	49.04 ± 0.96 f	9.01 ± 0.50 c	2.12 ± 0.13 ab	15.48 ± 1.40 b	13.79 ± 0.45 ab	SiL
I-C	> 105	4.91 ± 0.042 a	9.47 ± 0.25 c	7.78 ± 0.012 f	81.10 ± 2.14 d	7.40 ± 3.15 c	41.17 ± 1.82 c	45.57 ± 0.58 g	9.29 ± 0.26 c	1.85 ± 0.073 b	13.13 ± 1.46 c	13.88 ± 0.31 ab	SiL
II-A	0–10	5.09 ± 0.010 a	11.58 ± 0.45 a	25.6 ± 0.098 a	86.25 ± 2.40 a	12.38 ± 1.41 c	768.92 ± 9.00 a	125.16 ± 3.14 a	10.41 ± 0.46 a	8.69 ± 1.92 a	21.11 ± 0.42 b	5.30 ± 0.17 d	SiL
II-AB	10–30	4.90 ± 0.055 b	11.56 ± 0.34 a	15.06 ± 0.037 b	80.51 ± 1.64 b	55.42 ± 5.97 a	637.41 ± 7.34 b	75.47 ± 0.75 b	10.82 ± 0.43 a	7.26 ± 0.36 b	16.43 ± 1.94 cd	6.81 ± 0.15 b	SiL
II-B_1	30–50	4.85 ± 0.064 b	11.38 ± 0.23 a	10.42 ± 0.037 c	47.16 ± 2.18 d	5.19 ± 2.13 d	259.82 ± 10.32 d	49.62 ± 1.45 d	11.02 ± 0.21 a	3.18 ± 0.074 f	15.66 ± 0.72 d	7.48 ± 0.030 a	SiL
II-B_2	50–78	4.92 ± 0.044 b	11.22 ± 0.50 a	7.84 ± 0.098 d	44.88 ± 0.54 d	18.19 ± 1.21 b	328.65 ± 10.3 c	47.07 ± 0.19 d	10.78 ± 0.51 a	3.92 ± 0.23 e	18.16 ± 0.99 c	7.34 ± 0.12 a	SiL
II-B_3	78–100	5.09 ± 0.025 a	8.21 ± 0.44 b	5.63 ± 0.037 e	72.15 ± 1.58 c	52.37 ± 1.90 a	217.83 ± 5.49 e	62.34 ± 1.46 c	7.80 ± 0.44 b	4.94 ± 0.30 d	21.99 ± 1.28 b	6.44 ± 0.095 c	SiL
II-B_4	> 100	5.03 ± 0.010 a	4.34 ± 0.13 c	3.02 ± 0.098 f	41.92 ± 0.59 e	2.15 ± 0.12 d	179.30 ± 3.77 f	36.93 ± 1.22 e	4.08 ± 0.13 c	6.01 ± 0.12 c	28.19 ± 0.46 a	4.69 ± 0.026 e	SiL
III-A	0–8	4.69 ± 0.040 c	5.20 ± 0.38 b	10.06 ± 0.012 a	103.65 ± 5.18 b	11.20 ± 2.37 de	99.87 ± 3.48 a	82.28 ± 1.46 a	4.90 ± 0.39 b	5.73 ± 0.51 c	44.04 ± 0.88 e	8.46 ± 0.077 bc	L
III-B_1	8–24	4.78 ± 0.23 c	3.53 ± 0.20 ef	4.54 ± 0.037 b	109.61 ± 1.93 a	40.63 ± 0.49 bc	68.65 ± 1.59 b	77.42 ± 1.54 b	3.24 ± 0.20 de	8.41 ± 0.57 a	48.22 ± 2.98 d	7.77 ± 0.45 c	L
III-B_2	24–61	5.29 ± 0.061 ab	5.06 ± 0.19 bc	3.86 ± 0.17 c	62.02 ± 1.74 d	15.25 ± 1.86 d	70.81 ± 3.05 b	40.41 ± 0.55 g	4.87 ± 0.20 b	3.73 ± 0.22 e	40.33 ± 1.39 fg	10.42 ± 0.44 a	L
III-B_3	61–94	5.48 ± 0.049 a	6.45 ± 0.39 a	2.10 ± 0.098 d	71.02 ± 1.75 c	35.30 ± 1.51 c	74.92 ± 7.65 b	42.38 ± 0.85 g	6.22 ± 0.38 a	3.47 ± 0.16 ef	39.54 ± 0.54 g	10.30 ± 0.43 a	SiL
III-B_4	94–143	5.44 ± 0.035 a	6.78 ± 0.59 a	1.69 ± 0.073 ef	48.57 ± 0.87 e	38.60 ± 8.29 c	35.01 ± 2.71 gh	41.18 ± 0.73 g	6.61 ± 0.60 a	2.43 ± 0.41 g	42.55 ± 2.77 ef	10.69 ± 0.94 a	L
III-B_5	143–177	5.35 ± 0.021 ab	5.04 ± 0.13 bc	1.80 ± 0.085 e	43.33 ± 1.70 f	1.05 ± 0.22 f	34.12 ± 5.15 h	60.42 ± 1.39 e	4.90 ± 0.12 b	2.75 ± 0.10 fg	43.52 ± 1.99 e	10.57 ± 0.39 a	L
III-B_6	177–203	5.37 ± 0.020 a	4.46 ± 0.20 cd	2.19 ± 0.049 d	49.95 ± 3.24 e	38.52 ± 1.54 c	59.69 ± 7.53 c	59.59 ± 3.30 e	4.26 ± 0.18 bc	4.65 ± 0.16 d	49.95 ± 0.56 d	9.07 ± 0.27 b	L
III-B_7	203–222	5.44 ± 0.22 a	4.35 ± 0.33 d	1.61 ± 0.085 f	40.57 ± 0.99 fg	126.97 ± 5.41 a	46.76 ± 0.58 ef	55.25 ± 0.74 f	4.14 ± 0.44 c	6.12 ± 0.46 bc	58.99 ± 0.25 c	6.55 ± 0.17 d	SL
III-B_8	222–254	5.45 ± 0.049 a	3.91 ± 0.32 de	1.32 ± 0.012 g	42.98 ± 0.89 f	119.09 ± 8.34 a	42.00 ± 3.40 fg	56.50 ± 0.18 f	3.65 ± 0.31 cd	6.68 ± 0.30 bc	65.85 ± 1.56 b	5.32 ± 0.28 e	SL
III-B_9	254–278	5.32 ± 0.055 ab	3.19 ± 0.47 fg	1.22 ± 0.024 g	44.36 ± 1.52 f	48.42 ± 9.37 b	54.97 ± 1.78 cd	64.06 ± 1.23 d	2.98 ± 0.47 e	6.74 ± 1.11 b	71.36 ± 0.63 a	4.43 ± 0.46 f	SL
III-C	> 278	5.17 ± 0.066 b	2.82 ± 0.35 g	1.23 ± 0.012 g	37.31 ± 0.43 g	5.35 ± 2.82 f	50.53 ± 2.50 de	68.62 ± 0.23 c	2.66 ± 0.35 e	5.80 ± 0.66 bc	73.12 ± 1.07 a	4.60 ± 0.18 ef	SL
IV-A	0–7	4.46 ± 0.050 d	9.23 ± 0.17 a	20.15 ± 0.20 a	127.71 ± 1.44 a	42.63 ± 3.19 c	106.41 ± 1.37 c	101.03 ± 0.67 a	8.86 ± 0.17 b	4.09 ± 0.057 bc	53.48 ± 0.44 b	5.03 ± 0.10 f	SL
IV-AB	7–15	4.58 ± 0.025 c	6.68 ± 0.043 c	17.34 ± 0.024 b	110.38 ± 0.99 d	21.99 ± 4.43 e	80.57 ± 4.44 de	75.75 ± 0.65 b	6.39 ± 0.05 cd	4.32 ± 0.069 b	55.30 ± 0.77 a	5.61 ± 0.03 e	SL
IV-B_1	15–32	4.54 ± 0.021 c	7.46 ± 0.33 bc	13.41 ± 0.024 c	94.02 ± 2.46 ef	6.42 ± 0.33 f	90.88 ± 2.85 d	62.94 ± 0.78 c	7.21 ± 0.33 c	3.41 ± 0.20 d	52.41 ± 1.05 b	7.10 ± 0.16 d	SL
IV-B_2	32–59	4.92 ± 0.025 b	7.73 ± 0.45 bc	8.58 ± 0.037 d	117.77 ± 2.70 b	36.08 ± 0.71 d	87.09 ± 3.12 d	50.39 ± 0.41 e	7.44 ± 0.46 c	3.78 ± 0.28 cd	48.99 ± 0.96 c	8.06 ± 0.31 c	L
IV-B_3	59–81	5.03 ± 0.035 a	6.36 ± 0.63 c	4.65 ± 0.037 e	94.31 ± 1.52 e	129.97 ± 1.82 a	68.08 ± 2.27 f	40.34 ± 0.62 g	6.03 ± 0.63 d	5.27 ± 0.51 a	52.25 ± 0.67 b	8.36 ± 0.12 c	SL
IV-B_4	81–100	4.95 ± 0.049 b	10.10 ± 0.70 c	3.52 ± 0.12 g	82.70 ± 0.66 g	7.06 ± 1.86 f	72.71 ± 14.31 ef	41.85 ± 1.00 f	9.90 ± 0.70 a	2.03 ± 0.15 e	48.85 ± 0.68 c	10.34 ± 0.45 a	L
IV-B_5	100–125	4.97 ± 0.015 b	8.89 ± 1.17 a	3.71 ± 0.073 fg	114.27 ± 2.05 c	37.45 ± 0.58 d	142.51 ± 8.1 a	60.66 ± 1.09 d	8.53 ± 1.16 b	4.03 ± 0.49 bc	47.47 ± 2.14 c	10.31 ± 0.26 a	L
IV-B_6	>125	4.95 ± 0.015 b	10.80 ± 0.43 ab	3.91 ± 0.37 f	90.91 ± 1.86 f	107.20 ± 0.69 b	117.59 ± 2.94 b	51.53 ± 0.77 e	10.43 ± 0.43 a	3.40 ± 0.12 d	53.14 ± 0.66 b	8.79 ± 0.19 b	SL

Values with different lowercase letters are significantly different at the $P < 0.05$ level among the different soil layers of the same pedon

CEC cation-exchange capacity, SOM soil organic matter, BS base saturation, SiL silt loam, L loam, SL sandy loam

3.3 Soil shear properties

The shear properties of the soils are represented as the cohesive force and internal friction angle in Table 3. The cohesive force of the non-eroded soils was generally greater than that of the collapsed soils and ranged from 56.17 to 81.55 kPa (73.45 kPa on average) in the non-eroded soils and from 51.50 to 73.52 kPa (61.66 kPa on average) in the collapsed soils; the cohesion force of the non-eroded soils and the collapse soils was statistically significantly different ($P < 0.01$), indicating that non-eroded soils were better able to resist soil erosion from external forces. However, there were no significant differences in the internal friction angle between non-eroded soils and collapsed soils.

3.4 Scanning electron microscopy

The morphology of the clay particles in the soil samples was revealed to be hexagonal and elongated flakes (Fig. S1, Electronic Supplementary Material (ESM)). This morphology indicates that kaolinite is a major mineral in studied pedons. Kaolinite is a mineral with two types of surfaces, basal and edge, each of which has different surface properties and dimensions (Sayed Hassan et al. 2006). The pseudo-hexagonal plates with angular edges suggest that the kaolinite in the sample was also well crystallized. Particle shape is a fundamental feature of phyllosilicates and depends on the physicochemical conditions of geological crystallization, growth, transport, and deposition (Bergaya et al. 2006).

3.5 Powder and oriented X-ray diffraction analyses

The powder X-ray diffractograms of the sand and silt fractions indicated that feldspar, quartz, and ferrimagnetic magnetite (Fe_3O_4) were present. Quartz was the major component, with intense XRD reflection peaks at 3.34 and 4.26 Å. X-ray oriented diffraction patterns of the clay fractions of pedons I-B_4, II-B_3, III-A, and IV-A are shown in Fig. 3. The Mg-gly (the sample saturated with $MgCl_2$ and glycerol solvation) XRD pattern of all samples showed peaks at 14.1, 10.1, 7.1, 5.1, 4.85, 3.57, and 3.34 Å. In the Mg-saturated clay, the *d*-001 value was 14.1 Å and did not shift to higher *d*-spacing with glycerol solvation, indicating the absence of smectite in the soil clay fractions. The XRD pattern of K-saturated clay at 25 °C showed an XRD reflection peak at 14.1 Å and partly shifted toward 10.1 Å and completely disappeared after being heated to 350 °C. This response to heating indicates the loss of hydroxy-interlayer vermiculite (HIV) materials (Rich 1968; Barnhisel and Bertsch 1989; Chiang et al. 1999). The 10.1-, 5.1-, and 3.34-Å XRD reflection peaks remained unchanged after K-saturation and heat treatments, which indicates the presence of illite. The 7.1- and 3.57-Å XRD reflection peaks disappeared after heating to 550 °C, which indicates the presence of kaolinite. The 4.85-Å peak of the K-saturated sample disappeared after heating to 350 °C, which indicates the presence of gibbsite. A small, broad diffraction reflection between 14.1 and 10.1 Å (12.1 Å) in pedon I was detected in the K-saturated sample and disappeared after being heated to 550 °C, indicating the presence of a mixed layer in pedon I.

The results of the semi-quantitative analysis of clay minerals are shown in Table S1 (ESM) to illustrate the differences between the non-eroded and collapsed soils. Hydroxy-interlayered vermiculite (HIV), illite, kaolinite, and gibbsite ($Al(OH)_3$) were the major components in both non-eroded and collapsed soils. The amount of kaolinite in collapsed soils was greater than in non-eroded soils, which ranged from 71.4 to 86.9% in collapsed soils and 29.4 to 64.9% in non-eroded soils, while the content of HIV and gibbsite in non-eroded soils was greater than in collapsed soils. The HIV in the soils indicated that in the low SOM and moderate acidity environment with frequently wetting and drying cycles, the vermiculite interlayer hydroxyl species is an intermediate product of the weathering of 2:1 clay minerals to kaolinite (Rich 1968; Chiang et al. 1999). A large amount of kaolinite was present in the collapsed soil because the weathering intensity was enhanced due to greater leaching. Long periods of weathering and leaching can result in the formation of minerals such as kaolinite in Ultisols (Sanchez and Buol 1974).

3.6 Relationship between soil physicochemical properties and shear properties

Correlation between different soil physical and chemical properties of the study samples are shown in Table S2 (ESM). For the same forms of sesquioxides, Fe oxides showed significant positive relationships with Al oxides ($P < 0.05$). This result was similar to the findings of Wu et al. (2016). Moreover, sesquioxides had significant correlation with pH, CEC, SOM, $Al^{3+} + H^+$, and soil texture except Mn-oxides, but did not show significant correlation with K, Na, Ca, and Mg. For instance, Al_d had a significant positive correlation with Fe_d (0.934**), $Fe_d + Al_d$ (0.959**), Fe_o (0.649**), $Fe_o + Al_o$ (0.632**), Fe_p (0.597**), Al_p (0.618**), $Fe_p + Al_p$ (0.634**), CEC (0.818**), SOM (0.527**), exchangeable $Al^{3+} + H^+$ (0.823**), silt (0.931**), clay (0.500**), Fe_t (0.892**), and Fe_c (0.540**) and a significant negative correlation with Si_o (− 0.470**), Si_p (− 0.625**), pH (− 0.530**), and sand (− 0.936**).

Table 4 shows the relationship between the physicochemical properties of the soil samples and their shear properties. For all pedons, cohesive force had a significant positive correlation with Fe_d (0.669**), Al_d (0.774**), $Fe_d + Al_d$ (0.698**), Fe_o (0.536**), Al_o (0.508**), $Fe_o + Al_o$ (0.587**), Fe_p (0.519**), Al_p (0.544**), $Fe_p + Al_p$ (0.553**), CEC (0.814**), exchangeable $Al^{3+} + H^+$ (0.818**), silt (0.650**), clay (0.457**), and Fe_t (0.638**)

Table 3 Extractable Fe, Al, Si, and Mn concentrations and shear strength of studied pedons

Sample	Oxides types	Fe-oxides g kg^{-1}	Al-oxides	Si-oxides	Mn-oxides	Fe_t	$(Fe_d - Fe_o) \times 100 / Fe_d = Fe_c$ %	Cohesive force kPa	Internal friction angle °
I-A	d	34.80 ± 0.17 ab	11.13 ± 0.30 a	1.41 ± 0.53 a	0.40 ± 0.0063 f	46.63 ± 0.76 a	94.12 ± 0.66 b	79.55 ± 0.94 abc	33.99 ± 0.46 ab
	o	2.05 ± 0.23 a	2.19 ± 0.20 a	0.081 ± 0.0043 e	0.069 ± 0.0062 d				
	p	1.87 ± 0.48 a	1.85 ± 0.36 a	0.039 ± 0.0035 e	0.016 ± 0.0011 b				
I-B_1	d	35.18 ± 0.073 a	11.38 ± 0.32 a	0.78 ± 0.099 b	0.45 ± 0.0053 e	48.59 ± 1.25 a	94.19 ± 0.47 b	77.32 ± 0.83 bcd	34.43 ± 0.22 ab
	o	2.04 ± 0.16 a	2.24 ± 0.17 a	0.10 ± 0.0074 d	0.096 ± 0.0062 d				
	p	1.68 ± 0.15 a	1.87 ± 0.14 a	0.043 ± 0.0009 de	0.017 ± 0.00049 b				
I-B_2	d	35.37 ± 0.55 a	11.16 ± 0.34 a	0.97 ± 0.15 ab	0.57 ± 0.010 d	48.77 ± 2.42 a	95.87 ± 0.18 a	80.83 ± 0.96 ab	32.15 ± 0.64 c
	o	1.46 ± 0.043 b	1.79 ± 0.048 b	0.13 ± 0.0073 c	0.15 ± 0.0036 c				
	p	0.46 ± 0.070 b	1.18 ± 0.14 b	0.049 ± 0.0017 cde	0.030 ± 0.0023 a				
I-B_3	d	35.15 ± 0.34 a	11.46 ± 0.16 a	0.92 ± 0.087 ab	0.68 ± 0.0058 bc	48.56 ± 1.10 a	95.93 ± 0.36 a	81.55 ± 0.88 a	33.14 ± 0.82 bc
	o	1.43 ± 0.11 b	1.80 ± 0.094 b	0.16 ± 0.013 b	0.20 ± 0.0050 b				
	p	0.24 ± 0.022 b	1.03 ± 0.097 b	0.061 ± 0.011 bc	0.031 ± 0.0027 a				
I-B_4	d	34.32 ± 0.56 b	11.19 ± 0.52 a	0.76 ± 0.048 b	0.69 ± 0.028 b	48.63 ± 1.63 a	95.85 ± 0.29 a	75.85 ± 3.67 cd	34.41 ± 0.61 ab
	o	1.42 ± 0.095 b	1.79 ± 0.028 b	0.16 ± 0.0017 b	0.20 ± 0.0024 b				
	p	0.24 ± 0.010 b	1.03 ± 0.051 b	0.055 ± 0.0011 cd	0.030 ± 0.0015 a				
I-B_5	d	34.33 ± 0.51 b	10.82 ± 0.49 a	1.11 ± 0.56 ab	0.66 ± 0.028 c	46.84 ± 1.80 a	95.29 ± 0.29 a	73.46 ± 1.41 d	32.43 ± 0.40 c
	o	1.62 ± 0.079 b	1.89 ± 0.045 b	0.17 ± 0.0015 b	0.23 ± 0.0046 b				
	p	0.31 ± 0.015 b	1.16 ± 0.06 b	0.078 ± 0.013 a	0.032 ± 0.0007 a				
I-C	d	35.31 ± 0.21 a	11.17 ± 0.21 a	0.92 ± 0.084 ab	0.72 ± 0.012 a	46.94 ± 0.49 a	95.74 ± 0.31 a	61.27 ± 0.78 e	34.64 ± 0.37 a
	o	1.50 ± 0.12 b	1.84 ± 0.066 b	0.18 ± 0.0064 a	0.27 ± 0.040 a				
	p	0.36 ± 0.033 b	1.14 ± 0.084 b	0.069 ± 0.0071 ab	0.031 ± 0.0024 a				
II-A	d	36.86 ± 0.54 c	8.99 ± 0.13 b	0.99 ± 0.30 ab	0.37 ± 0.0061 a	62.48 ± 3.13 a	94.89 ± 0.15 e	74.13 ± 1.75 b	35.24 ± 0.10 a
	o	1.88 ± 0.061 b	1.36 ± 0.019 b	0.076 ± 0.0012 c	0.054 ± 0.00099 a				
	p	1.14 ± 0.10 a	1.24 ± 0.047 b	0.060 ± 0.0069 bc	0.023 ± 0.00056 a				
II-AB	d	37.40 ± 0.84 bc	10.10 ± 0.31 a	1.05 ± 0.42 ab	0.34 ± 0.0033 b	65.10 ± 1.08 a	94.34 ± 0.29 f	74.20 ± 1.12 b	33.36 ± 0.96 bc
	o	2.12 ± 0.065 a	1.60 ± 0.028 a	0.11 ± 0.0016 b	0.028 ± 0.0014 b				
	p	1.04 ± 0.020 b	1.45 ± 0.042 a	0.075 ± 0.0061 b	0.012 ± 0.0000058 a				
II-B_1	d	39.51 ± 0.76 a	10.41 ± 0.30 a	0.80 ± 0.15 b	0.32 ± 0.0026 de	63.51 ± 1.35 a	97.07 ± 0.12 d	78.80 ± 2.60 a	31.62 ± 0.45 c
	o	1.16 ± 0.068 c	1.36 ± 0.046 b	0.08 ± 0.0057 c	0.025 ± 0.00031 d				
	p	0.27 ± 0.020 c	0.98 ± 0.026 c	0.049 ± 0.0082 c	0.011 ± 0.000023 d				
II-B_2	d	38.43 ± 1.00 ab	10.21 ± 0.040 a	0.98 ± 0.10 ab	0.32 ± 0.0020 e	64.17 ± 3.40 a	97.89 ± 0.12 c	73.94 ± 0.38 b	32.35 ± 0.97 c
	o	0.81 ± 0.026 d	1.31 ± 0.033 b	0.11 ± 0.0020 b	0.026 ± 0.00050 c				
	p	0.12 ± 0.0007 d	0.91 ± 0.023 d	0.068 ± 0.020 bc	0.012 ± 0.000060 c				
II-B_3	d	39.27 ± 0.70 a	9.39 ± 0.12 b	1.04 ± 0.11 ab	0.33 ± 0.0067 bc	60.73 ± 0.47 a	98.82 ± 0.030 b	67.73 ± 1.73 c	34.19 ± 0.67 ab
	o	0.46 ± 0.0044 e	1.12 ± 0.024 c	0.15 ± 0.0055 a	0.024 ± 0.000086 de				
	p	0.070 ± 0.0062 de	0.85 ± 0.030 e	0.10 ± 0.012 a	0.011 ± 0.000034 d				
II-B_4	d	33.09 ± 0.68 d	6.89 ± 0.60 c	1.53 ± 0.71 a	0.33 ± 0.0062 cd	52.33 ± 2.92 b	99.19 ± 0.078 a	56.17 ± 1.91 d	29.35 ± 0.76 d
	o	0.27 ± 0.021 f	0.70 ± 0.041 d	0.075 ± 0.0028 c	0.023 ± 0.00033 e				
	p	0.031 ± 0.0023 e	0.56 ± 0.021 f	0.058 ± 0.0083 bc	0.011 ± 0.000054 d				
III-A	d	13.36 ± 0.14 e	3.93 ± 0.17 e	1.11 ± 0.46 b	0.38 ± 0.010 d	17.15 ± 2.55 e	88.12 ± 1.14 f	59.49 ± 2.42 bc	31.53 ± 1.45 a
	o	1.59 ± 0.17 a	1.66 ± 0.19 a	0.19 ± 0.021 cd	0.075 ± 0.0045 bc				
	p	0.073 ± 0.0059 a	0.96 ± 0.047 a	0.095 ± 0.0030 cd	0.030 ± 0.0013 d				
III-B_1	d	13.73 ± 0.24 e	3.13 ± 0.12 f	1.03 ± 0.020 b	0.44 ± 0.0034 c	16.83 ± 0.39 e	89.30 ± 0.71 ef	52.25 ± 6.47 de	25.19 ± 1.97 b
	o	1.47 ± 0.079 b	1.09 ± 0.050 e	0.17 ± 0.0036 d	0.11 ± 0.0020 bc				
	p	0.047 ± 0.0026 b	0.68 ± 0.045 cd	0.088 ± 0.0050 d	0.053 ± 0.0024 c				
III-B_2	d	21.99 ± 0.23 b	4.78 ± 0.037 c	1.28 ± 0.20 ab	1.12 ± 0.031 a	27.96 ± 0.44 b	94.75 ± 1.94 bc	56.61 ± 1.99 bcde	32.49 ± 0.33 a

Table 3 (continued)

Sample	Oxides types	Fe-oxides g kg^{-1}	Al-oxides	Si-oxides	Mn-oxides	Fe_t	$(Fe_d - Fe_o) \times 100 / Fe_d = Fe_c$ %	Cohesive force kPa	Internal friction angle °
	o	1.38 ± 0.031 b	1.46 ± 0.049 b	0.30 ± 0.091 a	0.48 ± 0.18 a				
	p	0.051 ± 0.0051 b	0.74 ± 0.053 bc	0.13 ± 0.0073 a	0.15 ± 0.013 a				
III-B_3	d	18.08 ± 0.72 d	4.50 ± 0.32 d	1.10 ± 0.092 b	0.48 ± 0.011 b	22.11 ± 1.03 d	95.99 ± 0.063 abc	63.21 ± 0.70 ab	34.95 ± 0.16 a
	o	0.72 ± 0.030 d	1.42 ± 0.088 bcd	0.30 ± 0.015 a	0.14 ± 0.0049 b				
	p	0.026 ± 0.0022 c	0.78 ± 0.022 b	0.12 ± 0.0065 ab	0.062 ± 0.0048 b				
III-B_4	d	18.07 ± 0.85 d	4.60 ± 0.062 cd	1.18 ± 0.058 ab	0.38 ± 0.0025 d	25.21 ± 1.79 c	96.18 ± 0.28 ab	55.17 ± 1.00 cde	34.01 ± 0.81 a
	o	0.69 ± 0.025 d	1.39 ± 0.079 bcd	0.29 ± 0.011 ab	0.075 ± 0.0032 bc				
	p	0.022 ± 0.0010 c	0.78 ± 0.043 b	0.12 ± 0.0028 ab	0.029 ± 0.0016 d				
III-B_5	d	19.94 ± 0.27 c	5.17 ± 0.085 b	1.15 ± 0.053 ab	0.35 ± 0.0012 e	24.14 ± 0.38 cd	95.75 ± 0.13 abc	68.15 ± 4.60 a	33.48 ± 0.46 a
	o	0.85 ± 0.029 c	1.44 ± 0.060 bc	0.32 ± 0.016 a	0.060 ± 0.0020 bc				
	p	0.023 ± 0.0012 c	0.68 ± 0.071 cd	0.10 ± 0.0075 c	0.025 ± 0.0023 d				
III-B_6	d	23.71 ± 0.90 a	5.80 ± 0.17 a	1.38 ± 0.055 ab	0.35 ± 0.0021 e	30.20 ± 1.30 a	97.06 ± 0.27 a	69.09 ± 1.51 a	33.99 ± 1.03 a
	o	0.69 ± 0.037 d	1.26 ± 0.043 d	0.32 ± 0.014 a	0.046 ± 0.0021 bc				
	p	0.024 ± 0.0017 c	0.62 ± 0.067 de	0.13 ± 0.0083 ab	0.015 ± 0.00054 e				
III-B_7	d	8.81 ± 0.52 f	3.09 ± 0.015 f	1.55 ± 0.43 a	0.28 ± 0.0012 fg	10.99 ± 1.37 f	94.55 ± 0.41 c	56.09 ± 3.39 bcde	31.76 ± 3.79 a
	o	0.48 ± 0.015 e	1.28 ± 0.018 cd	0.24 ± 0.0022 bc	0.027 ± 0.00024 c				
	p	0.015 ± 0.0005 d	0.60 ± 0.049 de	0.094 ± 0.005 cd	0.013 ± 0.00019 e				
III-B_8	d	5.62 ± 0.21 g	2.45 ± 0.066 g	1.12 ± 0.066 b	0.28 ± 0.016 f	15.31 ± 0.26 e	92.23 ± 1.04 d	51.50 ± 1.53 e	33.5 ± 0.064 a
	o	0.44 ± 0.064 ef	1.08 ± 0.18 e	0.19 ± 0.028 cd	0.025 ± 0.00081 c				
	p	0.017 ± 0.0013 d	0.65 ± 0.073 cde	0.10 ± 0.011 cd	0.013 ± 0.00042 e				
III-B_9	d	3.55 ± 0.11 h	2.02 ± 0.049 h	1.15 ± 0.13 ab	0.26 ± 0.00085 fg	4.89 ± 1.23 g	90.66 ± 0.48 e	58.12 ± 0.68 bcde	27.15 ± 0.52 b
	o	0.33 ± 0.018 f	0.97 ± 0.071 e	0.17 ± 0.0077 d	0.029 ± 0.00074 c				
	p	0.015 ± 0.0011 d	0.55 ± 0.039 e	0.12 ± 0.0066 b	0.015 ± 0.00044 e				
III-C	d	1.87 ± 0.18 i	1.71 ± 0.024 i	1.02 ± 0.21 b	0.26 ± 0.0013 g	3.99 ± 0.54 g	80.25 ± 0.74 g	59.00 ± 2.09 bcd	27.98 ± 0.26 b
	o	0.37 ± 0.021 ef	1.00 ± 0.055 e	0.17 ± 0.0082 d	0.026 ± 0.00029 c				
	p	0.017 ± 0.0017 d	0.56 ± 0.052 e	0.09 ± 0.013 cd	0.013 ± 0.00017 e				
IV-A	d	11.78 ± 0.058 de	5.12 ± 0.074 ab	1.26 ± 0.34 a	0.85 ± 0.015 f	15.63 ± 0.37 de	93.11 ± 0.42 c	55.34 ± 2.14 e	36.71 ± 0.45 a
	o	0.81 ± 0.046 bc	1.94 ± 0.030 ab	0.10 ± 0.0032 c	0.33 ± 0.031 d				
	p	0.25 ± 0.0202 a	1.42 ± 0.087 a	0.062 ± 0.011 bc	0.071 ± 0.0022 b				
IV-AB	d	11.27 ± 0.22 e	5.42 ± 0.57 a	1.14 ± 0.15 a	1.02 ± 0.017 e	15.29 ± 0.68 e	94.33 ± 0.57 b	63.10 ± 2.93 c	32.43 ± 1.23 c
	o	0.64 ± 0.053 d	1.73 ± 0.082 bc	0.11 ± 0.0050 c	0.38 ± 0.064 cd				
	p	0.14 ± 0.0083 b	1.22 ± 0.083 b	0.065 ± 0.013 bc	0.063 ± 0.0029 bc				
IV-B_1	d	12.25 ± 0.15 cd	5.23 ± 0.16 ab	1.17 ± 0.41 a	1.05 ± 0.034 e	16.36 ± 0.35 d	92.75 ± 0.31 c	61.80 ± 1.87 cd	34.98 ± 0.99 ab
	o	0.89 ± 0.028 b	1.94 ± 0.063 ab	0.13 ± 0.0046 b	0.42 ± 0.013 cd				
	p	0.097 ± 0.0106 c	1.24 ± 0.11 b	0.067 ± 0.0097 bc	0.071 ± 0.0064 b				
IV-B_2	d	11.80 ± 0.91 de	5.43 ± 0.16 b	1.10 ± 0.22 a	1.46 ± 0.017 a	17.41 ± 0.19 c	91.16 ± 0.25 d	73.52 ± 1.46 a	31.54 ± 0.18 c
	o	1.04 ± 0.059 a	2.17 ± 0.15 a	0.19 ± 0.012 a	0.77 ± 0.056 a				
	p	0.042 ± 0.0012 d	1.01 ± 0.047 c	0.058 ± 0.0027 c	0.072 ± 0.0052 b				
IV-B_3	d	12.66 ± 0.44 c	4.85 ± 0.046 bc	1.32 ± 0.40 a	1.39 ± 0.035 b	16.31 ± 0.35 d	94.11 ± 0.74 b	57.66 ± 2.06 de	32.08 ± 0.36 c
	o	0.75 ± 0.11 cd	1.65 ± 0.21 c	0.17 ± 0.018 a	0.54 ± 0.087 b				
	p	0.027 ± 0.0035 de	0.87 ± 0.12 c	0.082 ± 0.0081 ab	0.071 ± 0.0084 b				
IV-B_4	d	14.34 ± 0.44 a	5.00 ± 0.083 bc	1.09 ± 0.12 a	1.21 ± 0.025 d	19.55 ± 0.37 a	94.45 ± 0.77 b	73.07 ± 0.23 ab	31.83 ± 1.50 c
	o	0.80 ± 0.13 bc	1.74 ± 0.27 bc	0.19 ± 0.026 a	0.43 ± 0.069 c				
	p	0.025 ± 0.0008 e	0.90 ± 0.036 c	0.076 ± 0.010 abc	0.053 ± 0.0014 cd				
IV-B_5	d	13.55 ± 0.26 b	4.98 ± 0.056 bc	0.99 ± 0.068 a	1.26 ± 0.0068 c	18.47 ± 0.05 b	94.19 ± 0.27 b	68.36 ± 0.71 b	35.06 ± 0.66 ab
	o	0.79 ± 0.037 bc	1.68 ± 0.11 bc	0.19 ± 0.012 a	0.46 ± 0.027 bc				

Table 3 (continued)

Sample	Oxides types	Fe-oxides g kg^{-1}	Al-oxides	Si-oxides	Mn-oxides	Fe_t	$(Fe_d - Fe_o) \times 100 / Fe_d = Fe_c$ %	Cohesive force kPa	Internal friction angle °
IV-B_6	p	0.036 ± 0.0032 de	1.20 ± 0.16 b	0.094 ± 0.018 a	0.082 ± 0.0098 a	18.73 ± 1.13 ab	95.37 ± 0.30 a	70.01 ± 2.67 ab	33.43 ± 0.13 bc
	d	13.77 ± 0.12 ab	4.65 ± 0.16 c	1.03 ± 0.11 a	1.04 ± 0.026 e				
	o	0.64 ± 0.046 d	1.64 ± 0.11 c	0.17 ± 0.013 a	0.32 ± 0.037 d				
	p	0.022 ± 0.0015 e	0.89 ± 0.085 c	0.074 ± 0.014 abc	0.050 ± 0.0035 d				

Values with different lowercase letters are significantly different at the $P < 0.05$ level among the different soil layers of the same pedon

d free Fe-, Al-, Si-, and Mn-oxides; o X-ray non-crystalline Fe-, Al-, Si-, and Mn-oxides; p organically bound Fe-, Al-, Si-, and Mn-oxides

and a significant negative correlation with Si_d (− 0.493**), Si_p (− 0.571**), pH (− 0.452**), and sand (− 0.672**). The remaining soil parameters, i.e., Mn, exchangeable cations, and Fe_c, did not show significant correlations with cohesive force. The internal friction angle was correlated with Al_o (0.522**), Al_p (0.518**), CEC (0.532**), exchangeable Al^{3+} + H^+ (0.530**), and Fe_c (0.481**). For the non-eroded soils, the cohesive force showed a significant positive correlation with Al_d (0.683*), Fe_o (0.560*), Al_o (0.595*), Fe_o + Al_o (0.604*), CEC (0.850**), and exchangeable Al^{3+} + H^+ (0.860**). The correlation coefficients (R value) for cohesive force were greater than those for internal friction angle. In contrast, for collapsed soils, the internal friction angle had a significant positive correlation with Al_d (0.659**), CEC (0.586**), Al^{3+} + H^+ (0.589**), and Fe_c (0.628**), while the cohesive force had a significant positive correlation with Al_d (0.579**), CEC (0.554**), and Al^{3+} + H^+ (0.562*) but did not show a significant correlation with Fe_c.

Stepwise multiple linear regression analyses were performed to determine the dominant factor equations of shear properties (cohesive force (c) and internal friction angle (φ)). According to the relationships between cohesive force, internal friction angle, and physicochemical properties of the different pedons, the physicochemical properties had significant correlation with cohesive force and internal friction angle were selected as independent variables. The shear properties (cohesive force (c) and internal friction angle (φ)) of the different pedon groups were selected as the dependent variables, respectively, the cohesive force and internal friction angle of all pedons (c_1, φ_1), pedons I and II (non-eroded soils) (c_2, φ_2), and pedons III and IV (collapsing gully soils) (c_3, φ_3). The dominant factor equations were shown as follows:

$$c_1 = 2.490\left(Al^{3+} + H^+\right) + 47.487 \quad \left(r^2 = 0.818, P < 0.01\right) \tag{1}$$

$$\phi_1 = 0.421\,CEC + 29.334 \quad \left(r^2 = 0.532, P < 0.01\right) \tag{2}$$

$$c_2 = 2.982\left(Al^{3+} + H^+\right) + 43.525\left(r^2 = 0.860, P < 0.01\right) \tag{3}$$

$$\phi_2 = 0.976\left(Fe_o + Al_o\right) + 30.232\left(r^2 = 0.597, P < 0.05\right) \tag{4}$$

$$c_3 = 3.260\,Al_d + 47.617 \quad \left(r^2 = 0.579, P < 0.01\right) \tag{5}$$

$$\phi_3 = 1.545\,Al_d + 25.665 \quad \left(r^2 = 0.659, P < 0.05\right) \tag{6}$$

For all pedons, exchangeable Al^{3+} + H^+ was the dominant factor of cohesive force (Eq. (1)) and CEC was the dominant factor of internal friction angle (Eq. (2)). In non-eroded soils, exchangeable Al^{3+} + H^+ and Fe_o + Fe_o were the dominant factors affecting cohesive force (Eq. 3) and internal friction angle (Eq. (4)), respectively. In the collapsing gully soils, Al_d was the dominant factor affecting cohesive force (Eq. (5)) and internal friction angle (Eq. (6)).

4 Discussion

The reddish acid soils of Changting County contained low base saturation and exchangeable cations (Table 2). The CEC and exchangeable Al^{3+} + H^+ concentrations of the Changting red soils ranged from 2.82 to 12.96 cmol kg^{-1} and from 2.66 to 12.69 cmol kg^{-1}, respectively. The Fe_d concentrations of the non-eroded soils ranged from 33.09 to 39.51 g kg^{-1}, while the concentrations in the collapsing gully soils ranged from 1.87 to 23.71 g kg^{-1}; the concentrations of Al_d ranged from 6.89 to 11.46 g $kg^{-1}$and 1.71 to 5.80 g kg^{-1} of non-eroded and collapsed soils (Table 3). This was similar to the result of Xia et al. (2019), who reported the concentrations of Fe_d and Al_d in collapsing gully soils. High Fe_d and Al_d content usually indicated chemical weathering of silicates and the formation of Fe oxides (Zhang et al. 2017). It had been suggested that Fe- and Al-oxides play an important role in maintaining soil structural stability (Harris et al. 1966; Kemper and Koch 1966; Russell 1971). Fe_d content was higher than Al_d content, which might be ascribed to the higher density of the Fe co-precipitate than that of Al, the former not easily translocating with soil solution. Besides, Fe oxides tend to precipitate with other anions and coat the surface of fine particles (Kaiser and Guggenberger 2007). The cohesive force of the non-eroded soils ranged from 56.17 to 81.55 kPa and from 51.50 to 73.52 kPa in the collapsed soils, showing generally greater than that of the collapsed soils. These results indicated that sesquioxides and CEC have a significant impact on soil shear properties.

According to Tisdall and Oades' hierarchy theory (Tisdall and Oades 1982), sesquioxides stabilize aggregates at the micro-scale through cationic bridges or are bound with organic polymers, forming organo-mineral complexes. Sesquioxides are very dense and resistant to mechanical stress but are not stable under hydraulic stress (Zhou et al. 2012). Polyvalent Al^{3+} and Fe^{3+} cations can improve soil structure through cationic bridging and the formation of organo-metallic compounds and gels **(**Amézketa 1999**)**. Aggregates containing Al^{3+} and Fe^{3+} and high-CEC clays tend to have greater soil organic carbon (SOC) incorporation. The interaction of Al^{3+} and Fe^{3+} with kaolinite can synergistically promote aggregation with a limited impact on SOC (Six et al. 2000). However, oxides and hydroxides of Al^{3+} interact synergistically with SOC and dispersible clay to improve aggregate stability (Molina et al. 2001). Six et al. (2004) summarized that oxides can act as binding agents in three ways: by creating organo-mineral complexes, by enabling electrostatic binding between positively charged oxides and negatively charged clay minerals, and through developing a coat of oxides on the surface of minerals.

The correlation coefficients (*R* value) for CEC and exchangeable Al^{3+} + H^+ with cohesive forces were 0.814** and 0.818**, respectively, and with internal friction angles were 0.532** and 0.530**, respectively, showing high correlation and a significant difference ($P < 0.01$) with cohesive forces (Table 4). This finding indicated that in the acid soils, CEC and exchangeable Al^{3+} + H^+ concentrations played important roles related to cohesive forces. Moreover, stepwise multiple linear regression analyses results showed that exchangeable Al^{3+} + H^+ was the dominant factor of cohesive force both in all pedons and non-eroded soils. CEC and Fe_o + Al_o were the dominant factors of internal friction angle in all pedons and non-eroded soils, respectively. In the acid soils, H^+ can dissolve soil aluminum from soil minerals, forming Al^{3+} or H^+ clay (Hsu 1989). The CEC and exchangeable Al^{3+} + H^+ concentrations in the non-eroded soils were greater than those in the collapsing gully soils. This finding indicated that the acid soil CEC and exchangeable Al^{3+} + H^+ concentrations played more important roles in soil aggregation of the non-eroded soils than of the collapsing gully soils. While the results showed that Al_d were dominant factors affecting cohesive force and internal friction angle in the collapsing gully soils. Meanwhile, the results by Wang et al. (2016) revealed that Al_d was the most important binding agent and had prominent ability in aggregation of macro-aggregates.

The *R* values of the Fe_d correlations with cohesive forces and internal friction angles were 0.669** and 0.308, respectively, showing that Fe_d had a high correlation with cohesive forces but not with internal friction angles (Table 4). In all the statistical analyses, the *R* values of Fe_d correlations were higher than those of Fe_o and Fe_p. The high hydrolysis rates of iron are faster than those of Al; the iron forms precipitates with free Fe-oxides (Fe_d), X-ray non-crystalline Fe-oxides (Fe_o), and organic-bound Fe-oxides (Fe_p), coating the surface of clay and forming clay skins (Greenland and Hayes 1978; Schwertmann and Taylor 1989). In contrast, the low hydrolysis rates of Al form monomeric Al^{3+} plus H^+ ions in soil solutions, which then form Al^{3+}- or H^+-clay complexes (Hsu 1989). It has been suggested that SOM may promote soil aggregation through the following linkage: clay-(Al, Fe)-soil organic matter-(Al, Fe)-clay (Edwards and Bremner 1967).

The points of zero charge (PZC) of Si-gels, Mn-oxides, and SOM are near 2. The shear properties of red soils had poor correlations with Si-gels, Mn-oxides, and soil organic matter (SOM), including the Si_d, Si_o, Si_p, Mn_d, Mn_o, and Mn_p fractions (Table 4). The PZC of Al- and Fe-oxides range from 8 to 9.2 (Parks 1965). The permanent negative charge and CEC of kaolinite are low, at $x \approx 0$ and CEC ≈ 3 cmol kg^{-1} (Dixon 1989). Sesquioxides possess amphoteric properties (i.e., Fe_d) and can coat the surface of kaolinite and/or broken edges, neutralizing the surface charge (Dixon 1989; Schwertmann and Taylor 1989). The inert surface of quartz grains in a coarse soil cannot serve as cementing agents, resulting in low soil aggregation. Most SOM is negatively charged and is thus unlikely to react directly with clay particles, although it has been suggested that SOM enhances soil aggregation through

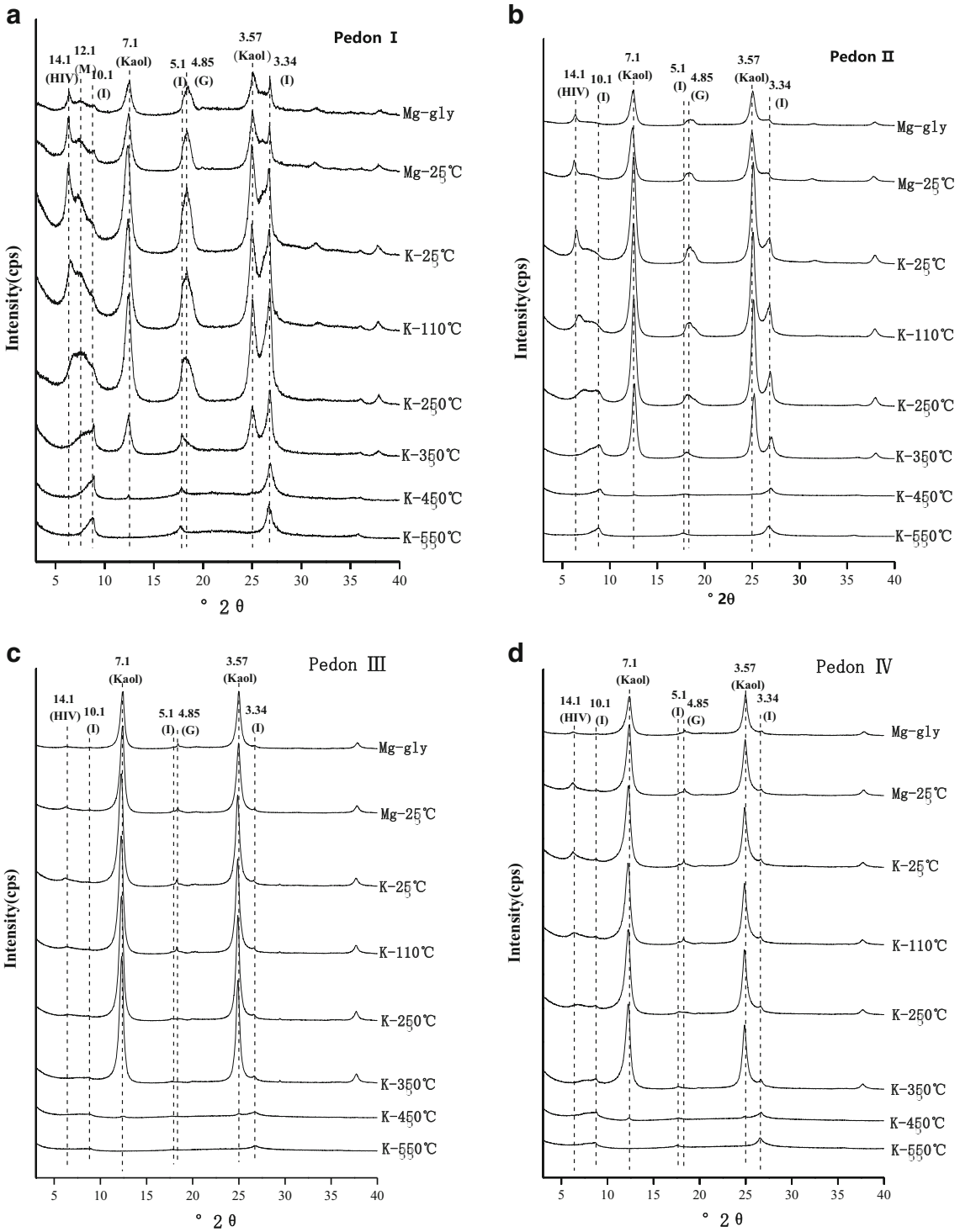

Fig. 3 X-ray diffraction patterns of the clays of **a** pedon I-B_4 (70–90 cm), **b** pedon II-B_3 (78–100 cm), **c** pedon III-A (0–8 cm), and **d** pedon IV-A (0–7 cm). HIV hydroxy-interlayered vermiculite, M mixed layer, I illite, Kaol kaolinite, G gibbsite

the formation of clay-sesquioxide-SOM-sesquioxide-clay complexes. The low SOM concentrations in the typical collapsed gullies should also be considered when assessing the influence of gibbsite or Fe-oxides/oxyhydroxides in soil aggregation.

El-Swaify and Emerson (1975) reported that $Al(OH)_3$ exerted little effect on soil aggregation at its PZC. In general, well-crystallized $Al(OH)_3$ may also be able to act as a cementing agent in acidic soil conditions, although the magnitude of this action may be negligible compared to that of X-

Table 4 Pearson's correlation coefficients between soil parameters and shear strength properties

Soil parameter	Shear property					
	Cohesive force			Internal friction angle		
	All pedon c_1	Pedon I and II c_2	Pedon III and IV c_3	All pedon φ_1	Pedon I and II φ_2	Pedon III and IV φ_3
Fe_d	0.669**	0.180	0.317	0.308	0.136	0.439
Al_d	0.774**	0.683*	0.579**	0.382*	0.500	0.659**
$Fe_d + Al_d$	0.698**	0.531	0.378	0.327	0.392	0.497*
Si_d	− 0.493**	− 0.446	− 0.250	− 0.109	− 0.480	0.206
Mn_d	0.038	0.111	0.467*	0.202	0.270	0.287
Fe_o	0.536**	0.560*	− 0.027	0.212	0.587*	− 0.103
Al_o	0.508**	0.595*	0.498*	0.522**	0.547	0.549*
$Fe_o + Al_o$	0.587**	0.604*	0.283	0.378*	0.597*	0.265
Si_o	− 0.324	− 0.035	0.145	0.038	0.273	0.158
Mn_o	− 0.001	0.056	0.446	0.167	0.279	0.250
Fe_p	0.519**	0.383	− 0.172	0.289	0.479	0.361
Al_p	0.544**	0.516	0.215	0.518**	0.555*	0.554*
$Fe_p + Al_p$	0.553**	0.438	0.146	0.402*	0.514	0.537*
Si_p	− 0.571**	− 0.418	− 0.248	− 0.117	0.093	− 0.043
Mn_p	− 0.274	0.206	0.091	0.135	0.313	0.257
pH	− 0.452**	− 0.642*	− 0.094	− 0.140	− 0.172	− 0.052
CEC	0.814**	0.850**	0.554**	0.532**	0.590*	0.586**
SOM	0.437*	0.470	− 0.019	0.400*	0.548	0.321
K	0.234	0.469	0.210	0.263	0.631*	0.167
Na	− 0.399*	− 0.025	− 0.301	− 0.012	0.196	0.040
Ca	0.269	− 0.040	0.364	0.165	0.151	0.321
Mg	0.166	0.446	− 0.266	0.141	0.558*	− 0.095
Al + H	0.818**	0.860**	0.562*	0.530**	0.561*	0.589**
Sand	− 0.672**	− 0.558*	− 0.253	− 0.347	− 0.436	− 0.433
Silt	0.650**	0.336	0.200	0.318	0.271	0.436
Clay	0.457**	0.362	0.248	0.333	0.275	0.363
Fe_t	0.638**	− 0.022	0.290	0.278	− 0.063	0.515*
Fe_c	0.338	− 0.547	0.268	0.481**	− 0.584*	0.628**

* and ** means correlation is significant at 0.05 level and 0.01 level (two-tailed)

ray non-crystalline materials. Fe-oxides show a stronger effect than those of $Al(OH)_3$ to crystallize. Thus, Fe-oxides are generally less effective than that of $Al(OH)_3$ in its cementing effectiveness except in frequently alternating oxidation and reduction cycles in soils. The $Al(OH)_3$ and Fe-oxides/oxyhydroxides in soils vary widely in their crystallinity and particle size, thus a poor correlation between their metal-oxide contents and aggregation. It is not necessarily indicated that they do not exert any effect on soil aggregation.

5 Conclusions

Compared to collapsing gully soils, non-eroded soils had superior physicochemical properties. For example, the non-eroded soils showed higher levels of CEC, Fe_t, Fe-, and Al-oxides than the collapsed soils. Additionally, the non-eroded soils contained more fine soil particles (silt and clay) than the collapsed soils, especially silt, while the collapsed soils had more sand. The shear properties showed that the cohesive force of the non-eroded soils was generally greater than that of the collapsed soils, indicating that non-eroded soils were better able to resist soil erosion from external forces. Furthermore, XRD analysis indicated that the studied soils contained HIV, illite, kaolinite, and gibbsite and that the amount of kaolinite in the collapsed soils was greater than that in the non-eroded soils. According to the correlation analyses of soil physicochemical properties and shear strength, CEC, exchangeable $Al^{3+} + H^+$, and sesquioxides had significantly positive correlations with cohesive force. The R value of

cohesive forces revealed a higher correlation with sesquioxide contents than internal friction angles. The stepwise regression analyses indicated that exchangeable $Al^{3+} + H^{+}$ and Al_d were the dominant factors affecting cohesive force. The results of this research provide some new insights into the relationship between shear strength and the soil physicochemical properties in the non-eroded soils and collapsing gully soils, and facilitate a better understanding of mechanism on the collapsing gullies. However, the internal friction angles of triaxial tests are related to soil particle size distribution, shape and arrangement, water contents, soil aggregation, etc. The shear strength of internal friction angles are more complicated than cohesive forces, thus merited further in-depth studies.

Acknowledgments Thanks are also extended to Zhi Zhang, Lizhen Su, Wenjing Wu, Xiaojing Si, Haiyan Tang, and Haidong Zhang for the assistance with sample analyses and Xiaojun Yan and Kai Yue for the soil sampling.

Funding information Funding was provided by the National Natural Science Foundation of China (No. 41571272) and the Co-Innovation Center for Soil and Water Conservation in Red Soil Region of the Cross-Straits, Fuzhou, China (No. K80ND800303).

References

Amézketa E (1999) Soil aggregate stability: a review. J Sustain Agric 14(2–3):83–151

Aniku JRF, Singer MJ (1990) Pedogenic iron oxide trends in a marine terrace chronosequence. Soil Sci Soc Am J 54(1):147–152. https://doi.org/10.2136/sssaj1990.03615995005400010023x

Barnhisel RI, Bertsch PM (1989) Chlorite and hydroxy-interlayered vermiculite and smectite. In: Dixon JB, Weeds SB (eds) Minerals in soil environments. Soil Sci. Soc. Am, Madison, pp 729–788

Bergaya F, Theng BKG, Lagaly G (2006) Handbook of clay science. Elsevier, Amsterdam

Brindley GW (1980) Quantitative X-ray mineral analysis of clays. In: Brindley GW, Brown G (eds) Crystal structures of clay minerals and their X-ray identification. Mineralogical society, monograph, no. 5 mineralogical society, London, pp 411-438

Chiang HC, Wang MK, Houng KH, White N, Dixon J (1999) Mineralogy of B horizons in alpine forest soils of Taiwan. Soil Sci 164(2):111–122

Dixon JB (1989) Kaolin and serpentine group minerals. In: Dixon JB, Weed SB (eds) Minerals in soil environments. Chapter 10, 2nd edn. Soil Sci Soc Am, Madison, pp 467–528

Dong Y, Wu Y, Yin J, Wang Y, Gou S (2011) Investigation of soil shear-strength parameters and prediction of the collapse of gully walls in the black soil region of northeastern China. Phys Geogr 32(2):161–178

Edwards AP, Bremner JM (1967) Microaggregates in soils. J Soil Sci 18(1):64–73

El-Swaify SA, Emerson WW (1975) Changes in physical properties of soil clays due to precipitated aluminum and iron hydroxides: I. Swelling and aggregate stability after drying. Soil Sci Soc Am 39(6):1056–1063

Ge H, Huang Y, Jiang F (2007) Geologic and geomorphologic conditions for slope collapse occurrences in Fujian. Bull Soil Water Conserv 27:128–132 (in Chinese with English abstract)

Greenland DJ, Hayes HB (1978) The chemistry of soil constituents. John & Wiley, New York, p 698

Harris RF, Chesters G, Allen N (1966) Dynamics of soil aggregation. Adv Agron 18:107–169

Hessel R, Van Asch T (2003) Modelling gully erosion for a small catchment on the Chinese loess plateau. Catena 54:131–146

Hsu PH (1989) Aluminum oxides and oxyhydroxides. In: Dixon JB, Weed SB (eds) Minerals in soil environments. Chapter 7, 2nd edn, Soil Sci Soc Am, Madison, pp 331–378

Imarhiagbe O, Williams CN (2014) Geotechnical parameters of gully erosion sites: a case study of the university of Benin erosion site. Nigerian Mining & Geosciences Society

Jackson ML (1979) Soil chemical analysis, 2nd edn. University of Wisconsin, Madison

Jiang F, Huang Y, Wang M, Lin JS, Zhao G, Ge HL (2014) Effects of rainfall intensity and slope gradient on steep colluvial deposit erosion in Southeast China. Soil Sci Soc Am J 78:1741

Kaiser K, Guggenberger G (2007) Distribution of hydrous aluminum and iron over density fractions depends on organic matter load and ultrasonic dispersion. Geoderma 140:140–146

Kakembo V, Xanga WW, Rowntree K (2009) Topographic thresholds in gully development on the hillslopes of communal areas in Ngqushwa Local Municipality, Eastern Cape, South Africa. Geomorphology 110(3–4):188–194

Kemper WD, Koch EJ (1966) Aggregate stability of soils from Western United States and Canada. Measurement procedure. Correlations with soil constituents. ARS, USDA Tech. Bull. No. 135

Le Roux JJ, Sumner PD (2012) Factors controlling gully development: comparing continuous and discontinuous gullies. Land Degrad Dev 23(5):440–449

Liggitt B, Fincham RJ (1989) Gully erosion: the neglected dimension in soil erosion research. S Afr J Sci 85(1):18–20

Lin J, Huang Y, Zhang D, Wang Y, Chen Q, Chen J, Wu X (2013) Influence of soil moisture content on shear characteristics of Benggang. J Soil Water Conserv 27:55–58 (in Chinese with English abstract)

Lin J, Huang Y, Wang MK, Jiang F, Zhang X, Ge H (2015) Assessing the sources of sediment transported in gully systems using a fingerprinting approach: an example from south-east China. Catena 129:9–17

Lin J, Zhu G, Wei J, Jiang F, Wang MK, Huang Y (2018) Mulching effects on erosion from steep slopes and sediment particle size distributions of gully colluvial deposits. Catena 160:57–67

Lohnes RA, Handy RL (1968) Slope angles in friable loess. J Geol 76(3):247–258

Luk SH, Peter D, Liu XZ (1997a) Water and sediment yield from a small catchment in the hilly granitic region, South China. Catena 29:177–189

Luk SH, Yao QY, Gao JQ, Zhang JQ, He YG, Huang SM (1997b) Environmental analysis of soil erosion in Guangdong Province: a Deqing case study. Catena 29(2):97–113

McKeague JA, Brydon JE, Miles NM (1971) Differentiation of forms of extractable iron and aluminum in soils. Soil Sci Soc Am J 35(1):33–38

Mehra OP, Jackson ML (1960) Iron oxide removal from soils and clays by a dithionite-citrate system buffered with sodium bicarbonate. Clay Clay Miner 7(1):317–327

Molina NC, Caceres MR, Pietroboni AM (2001) Factors affecting aggregate stability and water dispersible clay of recently cultivated semi-arid soils of Argentina. Arid Land Res Manag 15(1):77–87

Munro SD, Huang LJ (1997) Rainfall, evaporation and runoff responses to hillslope aspect in the Shenchong Basin. Catena 29(2):131–144

Okengwo ON, Okeke OC, Okereke CN, Paschal AC (2015) Geological and geotechnical studies of gully erosion at Ekwulobia, Oko and Nanka Towns, southeastern Nigeria. Electron J Geotech Eng 20(1):113–122

Okunlola IA, Abdulfatai IA, Kolawole LL, Amadi AN (2014) Geological and geotechnical investigation of gully erosion along River Bosso, Minna, north central Nigeria. J Geosci Geomatics 2(2):50–56

Pai C, Wang M, Wang W, Houng K (1999) Smectites in iron-rich calcareous soil and black soils of Taiwan. Clay Clay Miner 47(4):389–398

Parks GA (1965) The isoelectric points of solid oxides, solid hydroxides, and aqueous hydroxo complex systems. Chem Rev 65(2):177–198

Prosser IP, Slade CJ (1994) Gully formation and the role of valley floor vegetation, southeastern Australia. Geology 22:1127–1130

Rhoades JD (1982) Cation exchange capacity. In: Page AL (ed) Methods of soil analysis, 2nd edn. ASA and SSSA, Madison, pp 149–157

Rich CI (1968) Hydroxy interlayers in expansible layer silicates. Clay Clay Miner 16:15–30

Russell W (1971) Soil structure: its maintenance and improvement. J Soil Sci 22(2):137–151

Sanchez PA, Buol SW (1974) Properties of some soils of the Upper Amazon Basin of Peru1. Soil Sci Soc Am Proc 38:117–121

Sayed Hassan M, Villieras F, Gaboriaud F, Razafitianamaharavo A (2006) AFM and low-pressure argon adsorption analysis of geometrical properties of phyllosilicates. J Colloid Interface Sci 296(2): 614–623. https://doi.org/10.1016/j.jcis.2005.09.028

Schwertmann U (1964) Differenzierung der eisenoxide des bodens durch extraktion mit ammoniumoxalat-lösung. Zeitschrift für Pflanzenernährung, Düngung, Bodenkd 105:194–202

Schwertmann U, Taylor RM (1989) Iron oxides. In: Dixon JB, Weed SB (eds) Minerals in soil environments. Chapter 8, 2nd Ed., Soil Sci Soc Am, Madison, WI, pp 379–438

Sheng J, Liao A (1997) Erosion control in South China. Catena 29:211–221

Six J, Elliott ET, Paustian K (2000) Soil structure and soil organic matter: II. A normalized stability index and the effect of mineralogy. Soil Sci Soc Am 64:1042–1049

Six J, Bossuyt H, Degryze S, Denef K (2004) A history of research on the link between (micro)aggregates, soil biota, and soil organic matter dynamics. Soil Tillage Res 79(1):7–31

Tisdall JM, Oades JM (1982) Organic matter and water-stable aggregates in soils. J Soil Sci 33(2):141–163

Vincent C (2013) Impact of terrain attributes, parent material and soil types on gully erosion. Geomorphology 186:1–11

Wang J, Yang W, Yu B, Li Z, Cai C, Ma R (2016) Estimating the influence of related soil properties on macro- and micro-aggregate stability in Ultisols of south-central China. Catena 137:545–553

Wei J, Shi B, Li J, Li S, He X (2018) Shear strength of purple soil bunds under different soil water contents and dry densities: a case study in the Three Gorges reservoir area, China. Catena 166:124–133

Woo MK, Fang G, DiCenzo PD (1997) The role of vegetation in the retardation of rill erosion. Catena 29(2):145–159

Wu X, Cai C, Wang J, Wei Y, Wang S (2016) Spatial variations of aggregate stability in relation to sesquioxides for zonal soils, south-central China. Soil Tillage Res 157:11–22

Xia D, Deng Y, Wang S, Ding S, Cai C (2015) Fractal features of soil particle-size distribution of different weathering profiles of the collapsing gullies in the hilly granitic region, south China. Nat Hazards 79(1):455–478

Xia J, Cai C, Wei Y, Wu X (2019) Granite residual soil properties in collapsing gullies of south China: spatial variations and effects on collapsing gully erosion. Catena 174:469–477

Xu J (1996) Benggang erosion: the influencing factors. Catena 27:249–263

Xu X, Zhang Y, Jia D, Shu L (2011) U-Pb dating of volcanic rocks and granites along the Wuyishan Belt: constraints on tuning of Late Mesozoic tectonic events in Southeast China. Acta Geol Sin 85: 130–144

Zeng ZX (1960) The topography of rock. Geological Press, China (in Chinese)

Zhang Z, Huang L, Liu F, Wang M, Fu Q, Zhu J (2017) The properties of clay minerals in soil particles from two Ultisols, China. Clay Clay Miner 65(4):273–285

Zhong B, Peng S, Zhang Q, Ma H, Cao S (2013) Using an ecological economics approach to support the restoration of collapsing gullies in southern China. Land Use Policy 32:119–124

Zhou H, Peng X, Peth S, Xiao TQ (2012) Effects of vegetation restoration on soil aggregate microstructure quantified with synchrotron-based micro-computed tomography. Soil Tillage Res 124:17–23